A 2D Particle Velocity Sensor with Minimal Flow-Disturbance

Olti Pjetri, R.J. Wiegerink and G.J.M. Krijnen,
MESA+ Institute for Nanotechnology, University of Twente, The Netherlands, o.pjetri@utwente.nl

***Abstract*—A 2D sound particle velocity sensor, consisting of a cross of two connected, heated wires is presented. We developed a fabrication process by which the wires become freely suspended $350\,\mu m$ above the chip surface. This largely eliminates the influence of boundary layer effects and increases the temperature gradient along the wires, both due to the large distance to the silicon substrate. As a result, the sensor has increased sensitivity and reduced power consumption compared to an earlier design [1]. Furthermore, due to the fully symmetrical structure of the sensor the sensitive directions are exactly orthogonal to each other and have near identical sensitivity, thus requiring no individual calibration.**

I. Introduction

Particle velocity sensors based on thermal convection, either as single sensor or in combination with a microphone, have been used in the past for the measurement of one-, two- and three-dimensional sound intensities [1]–[6], acoustic impedances [7], [8], acoustic (in situ) absorption and pressure [9]. A widely used particle velocity sensor is the Microflown [10], [11]. It consists of three silicon nitride beams of $\approx 1\,mm$ length with a platinum layer on top. The central wire is electrically heated to about $600\,K$ while the two wires on the side act as temperature sensor by using the temperature dependent resistivity of the platinum [10]. In presence of a flow perpendicular to the wires, the temperature distribution will change asymmetrically leading to a temperature difference between the two sense wires. This temperature difference causes a change in resistance of the two sense wires which is a measure for the particle velocity. This principle has been extended to multiple dimensions by using multiple parallel wire configurations [12]–[14].

Traditionally, hot wire sound particle velocity sensors are based on parallel heated wires [15], where the particle velocity displaces the temperature profile perpendicular to the wires. Recently, we proposed a more robust crossed wire structure showing responsivity and bandwidth comparable with standard 1D particle velocity sensors [1]. The sensor provides for 2D particle velocity sensing with directivities aligned along each of the heated Pt wires using its temperature dependent resisitivity (fig 1). Initial designs were realized by removing a shallow part of the silicon underneath the sensor wires. Importantly, due to boundary layer effects the sensor-wires were not optimally exposed to the particle velocity field resulting in limitations in sensitivity and different sensitivity levels for the two directions.

In this work we present a new design in which the sensor-wires are suspended on a Si frame $350\,\mu m$ above the silicon surface (fig 2) thus eliminating the obstructions at the edges and minimizing boundary-layer effects both resulting in an increase of the particle velocity around the wires. The Si frame still has a very low thermal resistance, hence forcing room temperature at the edges of the sensor-wires and thus preserving high temperature gradients along each beam without obstructing the airflow. Furthermore, the support structures of the frame, which also have the bondpads on top, are also optimized to further increase the particle velocity at the position of the beams.

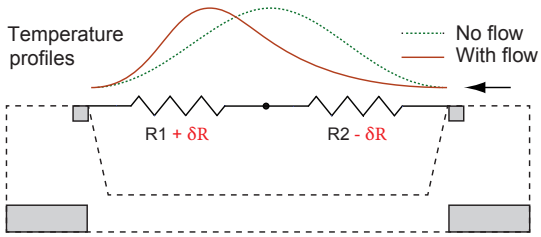

Fig. 1. Schematic of the working principle and vertical cut of the previous design (dashed line) where the wires are suspened above a $250\,\mu m$ deep pit in the wafer and the new design where the wires are suspended on a $5\,\mu m$ thick Si frame $350\,\mu m$ above the Si wafer (solid gray).

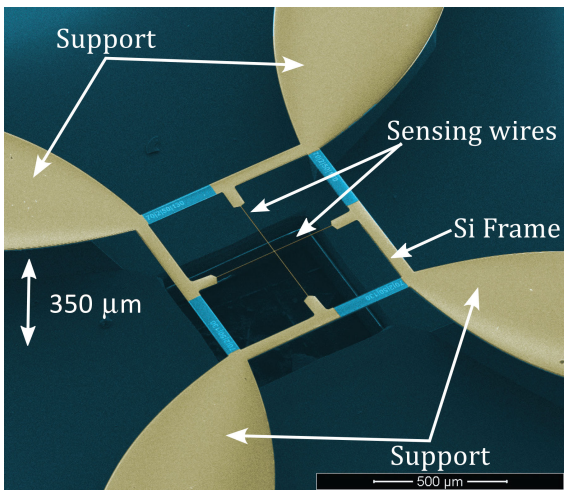

Fig. 2. False colored SEM photo of the new crossed wire particle velocity sensor. The sensor wires are elevated $350\,\mu m$ above the substrate improving particle velocity.

II. Design

The sensor consists of two silicon nitride wires of size $1000\,\mu m \times 2\,\mu m \times 0.15\,\mu m$ with a $150\,nm$ platinum layer on

978-1-4799-8203-5/15/$31.00 ©2015 IEEE

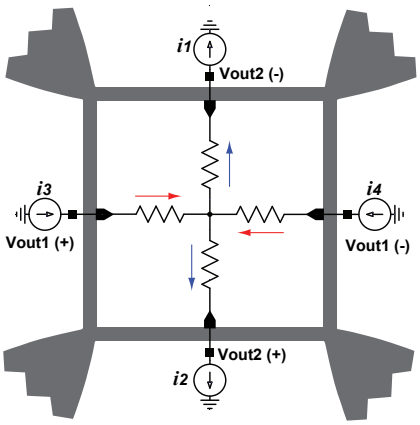

Fig. 3. Electrical interfacing using four (non-ideal) current sources. The current sources are implemented using matched transistor arrays in a current mirror topology.

top as shown in figure 2. The two wires act as both heaters and sensors using the temperature dependent resistance of the platinum layer. The wires are heated up to $\approx$600 K by injecting two currents with equal magnitude in both terminals of one of the wires and extracting them from the terminals of the other wire. The electrical interfacing is shown in figure 3 where both wires are depicted as two resistors in series making electrical connection at the center. In case of no flow, the temperature profile along each wire will be symmetrical resulting in equal resistance of the two parts of each wire as shown in figure 1. Because the currents injected through the terminals of each beam have equal magnitude but opposite directions, the voltage across each half of the wire will also have equal magnitude but opposite polarity leading to no voltage difference across the terminals of each wire. In the presence of a flow component in the direction parallel to a wire, the temperature profile along that wire will change asymmetrically leading to a different average temperature of the two halves of that wire which in turn causes a different electrical resistance of the two halves of the wire. This change in resistance gives rise to a voltage difference across the terminals of the wire which is a measure for the particle velocity component in the direction parallel to that wire.

Previous designs of the crossed wires particle velocity sensor consisted of the two wires suspended above a $250\,\mu\mathrm{m}$ potassium hydroxide (KOH) pit etched on the silicon wafer. A vertical cut of this design is shown by dashed lines in figure 1. This configuration presents several drawbacks. First, the particle velocity at the position of the wires is directly obstructed by the side walls of the pit. Furthermore, at these small scales the oscillatory boundary layer (also called "Stokes boundary layer") must be taken into account. The Stokes boundary layer refers to the boundary layer of an oscillatory flow close to a fixed surface where a no–slip condition holds. The amplitude of the oscillatory flow decreases when approaching the fixed surface until it becomes zero on the surface itself. The Stokes boundary layer is calculated by [16]:

$$\delta = 2\pi\sqrt{\frac{2\nu}{\omega}} \tag{1}$$

with ν being the kinematic viscosity of air ($\approx 1.5 \times 10^{-5}\,\mathrm{m^2\,s^{-1}}$ for dry air at room temperature) and ω the angular frequency of the motion (in $\mathrm{rad\,s^{-1}}$). At a distance δ from the fixed surface, the velocity amplitude has been reduced to $1 - e^{-2\pi} \approx 0.998$ times its value at free space. For dry air at room temperature, the Stokes boundary layer is calculated to be $\approx 430\,\mu\mathrm{m}$ at $1\,\mathrm{kHz}$ while reaching $\approx 1.37\,\mathrm{mm}$ at $100\,\mathrm{Hz}$. Second, the temperature gradient along the wires is also attenuated because the walls of the pit force room temperature relatively close to the wires. This attenuates the peak of the temperature profile at the center of the wires. Furthermore, these issues introduced by the walls become more severe with shorter wires.

The new design eliminates these two issues by suspending the wires on a $5\,\mu\mathrm{m}$ thick Si frame $350\,\mu\mathrm{m}$ above the Si wafer. A vertical cut of this new design is shown in solid gray in figure 1. The $5\,\mu\mathrm{m} \times 50\,\mu\mathrm{m}$ Si frame still has a very low thermal resistance, hence forcing room temperature at the edges of the sensor–wires and thus preserving high temperature gradients along each beam without obstructing the airflow. Both the airflow and temperature gradients along the wires are further improved by completely removing the silicon right underneath the wires.

Previous work [17] has shown that the specific mounting of the sensors can improve the signal by up to $11\,\mathrm{dB}$, an effect known as package gain. Here, we try to use this effect by designing the supports, which also have the bondpads on top, in the shape of horns, increasing the velocity of the air entering in between the supports when approaching the wires.

III. Experimental

A. Measurement setup

Fig 4 shows the measurement setup. We use the "piston-on-a-sphere" approach [18], [19] which exploits the known sound field in front of a loudspeaker placed in a spherical housing. Such a construction acts as an acoustic monopole on its center axis and has an accordingly acoustic impedance [19]. For high frequency measurements ($1\,\mathrm{kHz}$–$15\,\mathrm{kHz}$), the particle velocity sensor is placed at a distance of $25\,\mathrm{cm}$ from the loudspeaker and a pressure microphone is used to measure the pressure close to the sensor. The particle velocity at the position of the sensor is then calculated using the measured pressure close to the sensor and the known acoustic impedance of the acoustic monopole source. For low frequency measurements ($20\,\mathrm{Hz}$–$1\,\mathrm{kHz}$), the particle velocity sensor is placed very close to the speaker ($\approx$3 cm) while the pressure microphone is placed inside the spherical housing of the speaker. At low frequencies, the particle velocity close to the membrane is almost equal to the velocity of the membrane itself due to continuity conditions [19]. The velocity of the membrane itself can be calculated using the measured pressure inside the loudspeakers housing.

B. Responsivity measurements

The bare sensor die was mounted on a $4\,\mathrm{cm} \times 4\,\mathrm{cm}$ custom made printed circuit board containing all the necessary

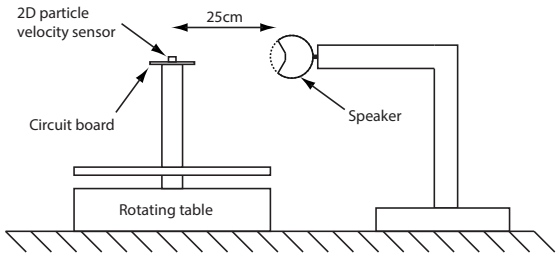

Fig. 4. Schematic of the measurement setup.

electronics for driving and readout of the sensor. The differential output of each wire is amplified using AD8421 low noise amplifiers with 1000× gain setting. The outputs of the amplifiers are captured with a Siglab 20-42 signal analyzer. For a more accurate result of both low– and high frequency measurements, 30 consecutive measurements were averaged. After merging the low– and high frequency measurements together, a Gaussian moving average filter with 16 samples was used to smooth the entire curve. The responsivity results are normalized with the specific impedance ρc. Instead of $\frac{V}{m/s}$, the results will be given in $\mathrm{V/P}a^*$ where 1 $\mathrm{P}a^*$ corresponds to $1\mathrm{P}a/\rho c \approx 2.4\,\mathrm{mm\,s^{-1}}$.

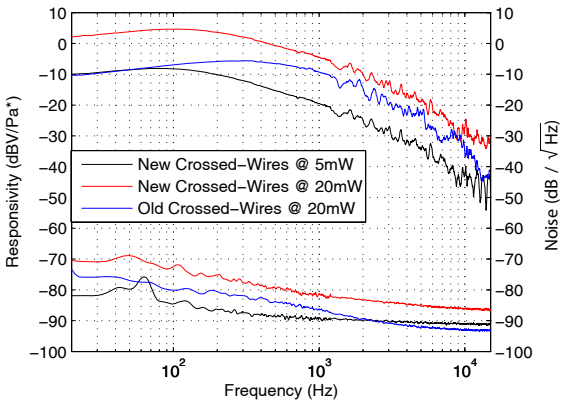

Fig. 5. Responsivity and noise curves of the previous and new sensor design at different total dissipated power.

C. Noise measurements

Noise measurements were performed by placing the bare sensor die and the PCB with the necessary electronics inside a $70\,\mathrm{cm} \times 70\,\mathrm{cm} \times 70\,\mathrm{cm}$ box filled with acoustic damping material and electromagnetically shielded. Each noise curve is obtained by averaging 100 consecutive autospectrum measurements with a Siglab 20-42 signal analyzer. Self noise curves relative to 94 dB free field are calculated from the responsivity and noise measurements. Fig 5 shows the frequency–response and noise of the previous crossed wires sensor with wire dimensions of $700\,\mathrm{cm} \times 2\,\mathrm{cm} \times 0.150\,\mathrm{cm}$ at 20 mW and the improved sensor at 5 mW and 20 mW. Selfnoise curves of three sensor designs operated at their maximum total dissipated power are shown in figure 6.

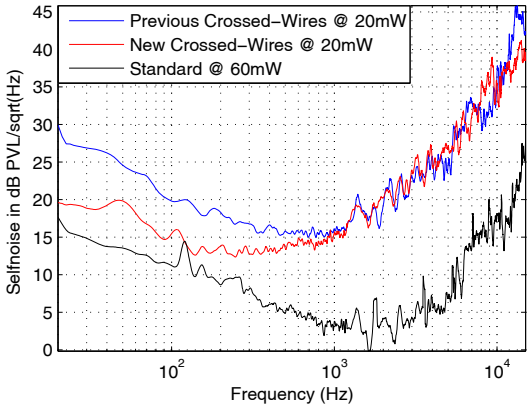

Fig. 6. Selfnoise curves of three sensor designs operated at their maximum total dissipated power.

D. Directivity measurements

For directivity measurements, the sensor was placed on a rotating table at a distance of 25 cm from the speaker. The speaker was driven by a single tone of 211 Hz using the internal generator of a lock-in amplifier. The differential outputs of both amplifiers were measured simultaneously using two different lock–in amplifiers. The rotating table and lock–in amplifiers were controlled using MATLAB. The directivity patterns of the previous asymmetrical sensor as well as the new design are shown in figure 7.

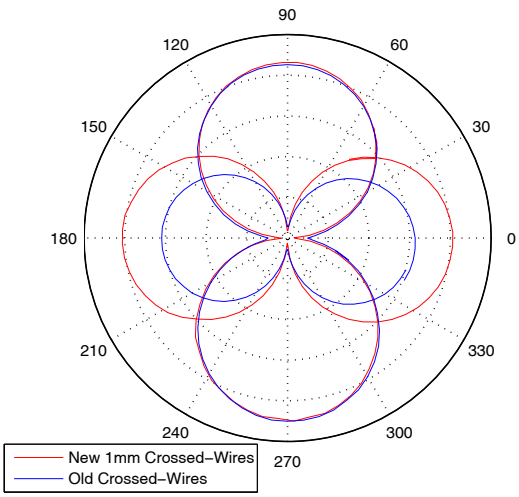

Fig. 7. Normalized directivity patterns along the directions of both wires, measured at 5 mW total power and at 211 Hz. The polar plots are scaled so that the largest lobes match.

IV. Discussion

The new design with suspended wires shows a decrease in selfnoise of up to 10 dB for low frequencies compared to the old design while at frequencies higher than ≈1 kHz, both designs show exactly the same selfnoise levels. This is due to higher sensitivity for low frequencies as can be seen in figure

5. While the noise curves of the old and new design show the same trend – despite the slightly higher noise level of the new design across the entire bandwidth – the sensitivity of these devices shows different trends. At frequencies higher than $1\,\mathrm{kHz}$ the sensitivity decays in the same fashion for both sensors while at frequencies lower than $1\,\mathrm{kHz}$ there is a clear shift in the corner frequency of these curves. This shift could be the result of oscillatory boundary layer effects in combination with the different geometries of the chips. At high frequencies, the boundary layer is thin compared to the characteristic lengths of the chip and the sensitivity is mostly determined by the heat capacity of the wires. At low frequencies however, the heat capacity becomes less important while the oscillatory boundary layer determines to a larger extend the particle velocity at the position of the wires. In the new design the wires are positioned at larger distance from the chip substrate hence the decrease in particle velocity at the position of the wires due the boundary layer effects will kick in at lower frequencies compared to the old design. However it must be noted that the wire lengths in the old and new design are also different ($700\,\mu\mathrm{m}$ versus $1000\,\mu\mathrm{m}$) hence quantitative conclusions with respect to the boundary layer effects can not be drawn from the present results.

V. Conclusions

The new sensor shows an improvement in sensitivity ranging between $5\,\mathrm{dB}$ at high frequencies to $12\,\mathrm{dB}$ at low frequencies when both sensors are operated at $20\,\mathrm{mW}$ total power. Furthermore, the selfnoise of the new design is up to $10\,\mathrm{dB}$ lower compared to the old design at frequencies lower than $1\,\mathrm{kHz}$.

The standard parallel wire particle velocity sensor provides better selfnoise performance, however it dissipates six times more power per direction (1D) compared to the new crossed wires design.

Finally, the directivity patterns of both crossed wires designs show an almost perfect figure of eight and excellent orthogonality of the two directions. Contrary to the old design however, the new sensor shows almost equal sensitivity in both directions.

Acknowledgment

The authors would like to thank provinces Gelderland and Overijssel for supporting this project in the GO EFRO program. Furthermore, the authors gratefully acknowledge Doekle Yntema for his help with measurements and calibration, Kechun Ma for help with the cleanroom work, Meint de Boer and Erwin Berenschot for their contribution to the fabrication process.

References

[1] O. Pjetri, R. Wiegerink, T. Lammerink, and G. Krijnen, "A crossed-wire 2-dimensional acoustic particle velocity sensor," in *SENSORS, 2013 IEEE*, Nov 2013, pp. 1–4.

[2] H.-E. de Bree, W. F. Druyvesteyn, E. Berenschot, and M. Elwenspoek, "Three-dimensional sound intensity measurements using microflown particle velocity sensors," in *Proc. Twelfth IEEE Int. Conf. Micro Electro Mechanical Systems MEMS '99*, 1999, pp. 124–129.

[3] H.-E. de Bree, W. F. Druyvesteyn, and M. Elwenspoek, "Realisation and calibration of a novel half inch p-u sound intensity probe," in *Audio Engineering Society Convention 106*, 5 1999.

[4] W. F. Druyvesteyn, H.-E. de Bree, and M. Elwenspoek, "A new acoustic measurement probe the microflown," in *Proceedings of the Institute of Acoustics*, The Barbican, London, England, 1999, pp. 140–147.

[5] W. F. Druyvesteyn and H.-E. de Bree, "A new sound intensity probe: Comparison to the brüel & kjaer p-p probe," in *Audio Engineering Society Convention 104*, 5 1998.

[6] O. Pjetri, R. J. Wiegerink, T. S. J. Lammerink, and G. J. M. Krijnen, "A novel two dimensional particle velocity sensor," in *International Congress on Acoustics, Montreal, Canada*. Acoustical Society of America, June 2013, pp. 1–6.

[7] H. Schurer, P. Annema, H. elias De Bree, C. H. Slump, and O. E. Herrmann, "Comparison of two methods for measurement of horn input impedance," in *Proc. 100th AES Convention*, Copenhagen, Denmark, 1996.

[8] F. van der Eerden, H.-E. de Bree, and H. Tijdeman, "Experiments with a new acoustic particle velocity sensor in an impedance tube," *Sensors and Actuators A: Physical*, vol. 69, no. 2, pp. 126–133, August 1998.

[9] H.-E. de Bree, T. Korthorst, P. Leussink, H. Jansen, and M. Elwenspoek, "A method to measure apparent acoustic pressure, flow gradient and acoustic intensity using two micromachined flow microphones," in *Proceedings Eurosensors X*, Leuven, Belgium, 1996, pp. 827–830.

[10] H.-E. de Bree, P. Leussink, T. Korthorst, H. Jansen, T. Lammerink, and M. Elwenspoek, "The μ-flown- a novel device measuring acoustical flows," in *Proc. and Eurosensors IX. Solid-State Sensors and Actuators Transducers '95. The 8th Int. Conf*, vol. 1, 1995, pp. 536–539.

[11] H.-E. de Bree, "Use of a fluid flow measuring device as a microphone and system comprising such a microphone," in *Patent PCT/NL95/00 220*, 1996, pp. 124–129.

[12] D. Yntema, R. Wiegerink, J. van Honschoten, and M. Elwenspoek, "Fully integrated three dimensional sound intensity sensor," in *Micro Electro Mechanical Systems, 2007. MEMS. IEEE 20th International Conference on*, Jan 2007, pp. 51–54.

[13] D. Yntema, J. van Honschoten, and R. Wiegerink, "An integrated 3d sound intensity sensor using four-wire particle velocity sensors: I. design and characterization," *Journal of Micromechanics and Microengineering*, vol. 20, no. 1, pp. 1–7, 2010. [Online]. Available: http://doc.utwente.nl/69830/

[14] J. W. van Honschoten, D. R. Yntema, and R. J. Wiegerink, "An integrated 3d sound intensity sensor using four-wire particle velocity sensors: Ii. modelling," *Journal of Micromechanics and Microengineering*, vol. 20, no. 1, p. 015043, 2010. [Online]. Available: http://stacks.iop.org/0960-1317/20/i=1/a=015043

[15] J. van Honschoten, V. B. Svetovoy, G. J. Krijnen, and M. C. Elwenspoek, "Optimization of a thermal flow sensor for acoustic particle velocity measurements," *Journal of Microelectromechanical Systems*, vol. 14, no. 3, pp. 436–443, 2005. [Online]. Available: http://doc.utwente.nl/52575/

[16] G. K. Batchelor, *An introduction to fluid dynamics*. Cambridge University Press, 2000.

[17] J. van Honschoten, D. Yntema, M. Dijkstra, V. Svetovoy, R. Wiegerink, and M. Elwenspoek, "Analysis of packaging effects on the performance of the microflown," in *Proceedings of DTIP of MEMS & MOEMS 2006*. Grenoble: TIMA Editions/DTIP, April 2006. [Online]. Available: http://doc.utwente.nl/66903/

[18] F. Jacobsen and V. Jaud, "A note on the calibration of pressure-velocity sound intensity probes," *Acoustical Society of America. Journal*, vol. 120, no. 2, pp. 830–837, 2006, copyright (2006) Acoustical Society of America. This article may be downloaded for personal use only. Any other use requires prior permission of the author and the Acoustical Society of America.

[19] T. G. H. Basten and H.-E. de Bree, "Full bandwidth calibration procedure for acoustic probes containing a pressure and particle velocity sensor," *The Journal of the Acoustical Society of America*, vol. 127, no. 1, pp. 264–270, 2010. [Online]. Available: http://scitation.aip.org/content/asa/journal/jasa/127/1/10.1121/1.3268608